JCTC Journal of Chemical Theory and Computation

Article

pubs.acs.org/JCTC

Computational Protocol for Modeling Thermochromic Molecular Crystals: Salicylidene Aniline As a Case Study

Davide Presti,[†] Fréderic Labat,[‡] Alfonso Pedone,*[,†] Michael J. Frisch,[§] Hrant P. Hratchian,[∥] Ilaria Ciofini,[‡] Maria Cristina Menziani,[†] and Carlo Adamo*[,‡,⊥]

[†]Dipartimento di Scienze Chimiche e Geologiche, Università di Modena e Reggio-Emilia, 183 via G. Campi, I-41125 Modena, Modena, Italy

[‡]Institut de Recherche de Chimie Paris CNRS, Chimie ParisTech, 11 rue P. et M. Curie, F-75005 Paris 05, France

[§]Gaussian, Inc., 340 Quinnipiac Street, Building 40, Wallingford, Connecticut 06492, United States

[∥]Chemistry and Chemical Biology, University of California, Merced, California 95343, United States

[⊥]Institut Universitaire de France, 103 Boulevard Saint Michel, F-75005 Paris, France

Supporting Information

ABSTRACT: A computational protocol that combines periodic and QM/QM′ calculations has been applied to investigate the structural (geometrical and electronic) and photophysical absorption properties of the salicylidene aniline (SA) thermochromic molecular crystal. The protocol consists of three different steps, namely (i) the description of the molecular crystal using a periodic approach taking into account dispersion interactions, (ii) the identification of reliable finite models (clusters), and (iii) the calculation of vertical transition energies including environmental effects through the use of an electronic embedding model (QM/QM′ ONIOM approach). The encouraging results obtained in this work for the β polymorph of SA, both in terms of accuracy and computational cost, open the way to the simulation and the prediction of the photophysical behavior of other molecular crystals, especially those much less well characterized experimentally.

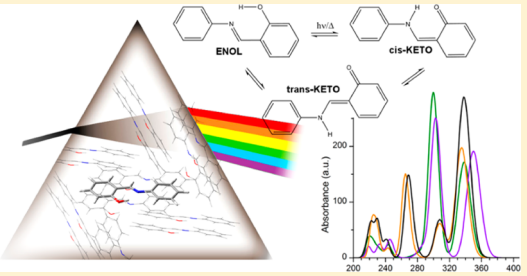

1. INTRODUCTION

Thermochromic (TC) and photochromic (PC) organic molecular crystals, that is, systems that change their color by thermo- or photoirradiation, have recently attracted much interest in nanotechnology and optoelectronics due to their potential technological applications such as data storage, electronic display systems, optical switching devices, and actuators.[1−6] For more than a century (see first reports collected in refs 7 and 8), molecular and solid Salicylidene Aniline (SA, Figure 1) and its derivatives have been extensively investigated through the use of different spectroscopic techniques (such as UV−visible absorption and emission spectroscopies[9−20]).

Notwithstanding SA shows a simple structural behavior, it presents manifold PC/TC mechanisms. Briefly explained, SA is a system that exhibits an excited-state intramolecular proton transfer (ESIPT) of the hydroxyl proton transforming from the − colorless − cis-enol form to the corresponding − colored − cis-keto tautomer. The ESIPT reaction can be photo- or thermically induced.[15,20,21] Successive to the proton transfer (PT), a cis−trans isomerization of the keto form takes place, yielding to the final orange-red colored photoproduct. From these detailed experimental investigations, some points have been clearly established: i) it was demonstrated that the pale-yellow color first attributed to the stable enol form of molecular SA within all the solid phases is actually related to the presence

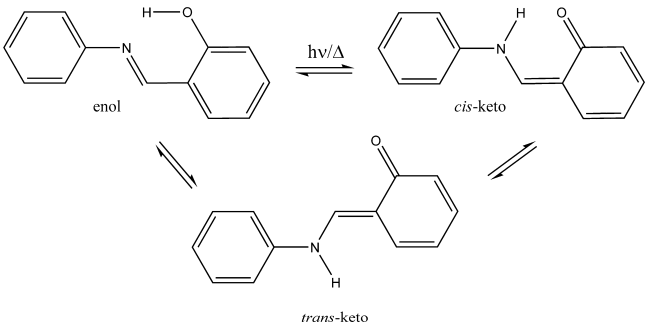

Figure 1. Schematic illustration of ESIPT process in SA: the ground-state enol-form, when excited by photo- or thermoirradiation, undergoes the ESIPT process resulting in the cis-keto form. The latter can give a cis−trans photoisomerization to the metastable trans-keto form or relax back.

of traces of the unstable cis-keto form at room temperature.[14] Therefore, it is nowadays accepted that ideal, stable, and pure crystals (of any phase) of SA in the enol form are colorless; ii) two PC structures, namely α_1[22,23] and α_2,[23,24] and one TC (β[23]) polymorph were obtained and investigated. Nonetheless after the structural revision of Arod et al.,[23] no experimental

Received: September 27, 2014

   dx.doi.org/10.1021/ct500868s | J. Chem. Theory Comput. XXXX, XXX, XXX−XXX

investigations of the PC/TC properties of SA in solid state are available, with the mechanisms and energetics of this PC/TC induced processes still unknown, as well as the crystal structure of the ESIPT products (that is the cis-keto or trans-keto tautomers).

On the theoretical side, isomerization and photoisomerization of SA have been deeply investigated using different computational approaches, albeit all the works were focused on the molecular aspects (see refs 21, 25, and 26 for recent efforts on this topic). More generally, recent articles have shown that is indeed, nowadays, possible to describe quite accurately the excited state proton transfer phenomena at the molecular level[27−29] using both post-Hartree−Fock and Density Functional Theory (DFT) based approaches. Nonetheless, situations dealing with the properties of these compounds in condensed phases and, particularly, in solid-state are much more involved.[14,23,30]

In order to define a general computational protocol enabling the description of the different polymorphs of photo- and thermochromic molecular crystals, both from a geometrical, electronic, and spectroscopic point of view, SA can be considered as an excellent test case, in view of the detailed experimental characterization mentioned above. Due to the complexity of PC/TC mechanisms at work in crystalline SA, we decided to focus, in this work, on the computational investigation of the β thermochromic polymorph. In particular, we aim to define a DFT based computational approach to enable the description of the structural and optical − here UV−vis absorption − features of such a molecular crystal.

This type of protocol relies on a periodic DFT description of the structural and electronic features of the molecular crystal at the ground state. It makes use of corrections to deal with the presence of dispersion interactions and of a Time-Dependent DFT (TD-DFT) QM/QM′ ONIOM embedding model[31−33] to reproduce the influence of the surroundings on the UV−vis properties of the SA.

Indeed, assuming that the enol-to-cis-keto PT process and, in the same way, the cis−trans (keto) isomerization *do not* take place *simultaneously* for all the molecules in the crystal, but that these processes take place locally first, it is possible to spectroscopically characterize the photo- or thermally induced proton transfer using a cluster model. In particular, by cutting out from the molecular bulk crystal representative clusters containing all relevant surrounding molecules, the ground and excited state properties of all species involved in the PT reaction can be computed and the properties of the molecular material simulated. It should be noticed that a previous theoretical study focused on the investigation of excited-state geometries of molecular crystals, using a QM/MM approach.[34] However, such a study did not consider periodic DFT calculations for the solid state phase, and the MM level can be considered as insufficient for mimicking the surrounding effects on the local excited state, especially when electronic embedding is missing.

The considerations made above thus allow the setup of a mixed periodic/cluster approach to study the PT mechanism, provided that the same DFT computational level can be applied.

DFT, especially in conjunction with the use of hybrid functionals, has indeed proven to be a powerful tool for the description of electronic and structural features of bulk materials (both crystals[35] and molecular crystals[36−38]), and the recent implementation of corrections to take dispersion interactions into account have further strengthened its accuracy.[39] At the same time the efficient implementation of embedding techniques in an ONIOM formalism, by allowing the simulation of the effect of the surroundings on ground (DFT) and excited (TD-DFT) states at the molecular level, provides all the necessary building blocks for the setup of an efficient and accurate computational protocol for the description of ground and excited state properties of photochromic molecular crystals.

The paper is organized as follows: after the computational details (Section 2), a discussion of the ground state structural and electronic features computed for the different isomers of SA in solid, solution, and gas-phase is given (Section 3). Next, vertical excited states are computed in gas-phase, solution, and solid state (through the use of a QM/QM′ approach), and the results obtained are compared with the available experimental data. Finally, some general conclusions are drawn.

2. COMPUTATIONAL DETAILS

Ground State Periodic Calculations. A parallel version of the CRYSTAL09 package,[40,41] within the frame of all-electron atom-centered Gaussian basis sets, was employed for ground-state calculations of bulk molecular crystals. After checking convergence on the Monkhorst−Pack *k*-points grid, we set the number of *k*-points to 27, in the Irreducible Brillouin Zone (IBZ). The DFT grid consisted of 75 radial and 974 angular points. The tolerances on bielectronic integrals (Coulomb and Exchange series) were set to 10^{-7}, 10^{-7}, 10^{-7}, 10^{-7}, and 10^{-18}.

A full geometry optimization − both of cell parameters and atomic displacements − of the enol-form of the β polymorph of SA was carried out at the B3LYP, B3LYP-D2, and B3LYP-D* level of theory starting from the experimental structure,[23] imposing periodic boundary conditions (PBC) and using default convergence criteria on gradients and atoms displacements.

We decided to adopt the B3LYP functional[42,43] because it is well-known that hybrid functionals describe the ground and excited states − ex. valence excitations − of molecular systems with 20% to 40% accuracy.[44] In general, they also provide a correct description of hydrogen bonding. The -D2[45] and -D*[46] *a posteriori* dispersion-correction terms have been used since other more recent and accurate schemes (i.e[46] −D3,[47] TS,[48] MBD,[49] and XDM[50]) are not available in the present version of the CRYSTAL code. It is worth highlighting that the -D* consists of a modified version of the Grimme -D2 scheme, especially devised for molecular crystals.

Three basis sets (namely the 6-311G(d), 6-311G(d,p), and pob-TZVP basis sets[51,52]) were tested in conjunction with the B3LYP functional. Based on Single Point energy results (convergence of energy, computational cost) and on previous structural optimizations (convergence of energy, cost and accuracy in predicting lattice constants), the 6-311G(d) basis set was selected for full geometry optimizations − since it represents a good balance between quality of the results and computational cost.

Excited State QM/QM′ Calculations. A cluster of 15 molecules of SA was extracted from the fully optimized crystal in the enol form to be used for ONIOM QM/QM′ calculations. One SA molecule was treated at high-level (QM layer), while 14 molecules were kept at low-level (QM′ layer). The innermost SA molecule (high-level) was fully optimized with CRYSTAL09 (B3LYP-D*/6-311G(d)), keeping fixed the coordinates of surrounding molecules. The same optimization

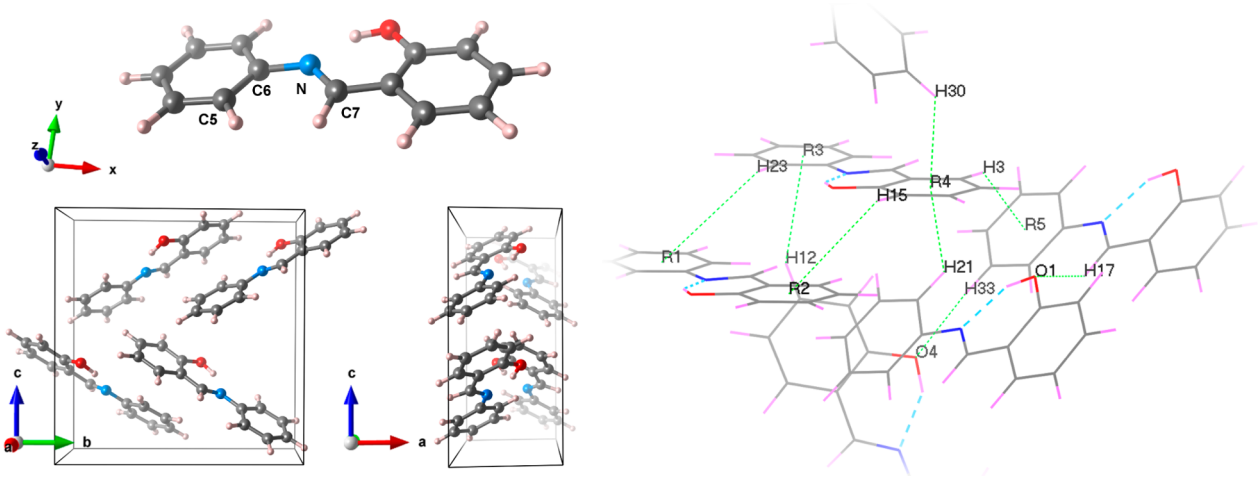

Figure 2. Representation of the SA molecule: Left (top): the SA molecule in its almost-planar configuration inside the crystal. (bottom): view of the *bc* plane and *ac* plane of the unit cell. Right: Intermolecular parameters (green lines) of β polymorph. A labeling for involved atoms is given. Intramolecular H-bonds are highlighted with blue lines.

Table 1. Cell Parameters (Å), Volume (Å^3), and Percentage Relative Volume Deviations with Respect to the Experimental Data (*Rel. Vol. Dev. %*) Computed for the Fully Optimized β Polymorph of SA[b]

	B3LYP	B3LYP-D2	B3LYP-D*	exp.[a]
a	6.846 (1.052)	5.589 (−0.205)	5.755 (−0.039)	5.794
b	11.855 (−1.163)	12.476 (−0.542)	12.781 (−0.237)	13.018
c	18.111 (4.494)	12.720 (−0.897)	13.141 (−0.476)	13.617
volume	1469.829	886.934	966.651	1027.077
Rel. Vol. Dev. %	+43.11	−13.65	−5.88	

[a]From ref 23 measured at T = 120 K. [b]Deviations are reported in parentheses.

procedure was pursued, maintaining fixed the low-level layer in the enol form, while fully relaxing the central molecule in its cis-keto or trans-keto forms. The clusters obtained are labeled, for convenience, in the following as **C-enol**, **C-cis-keto**, and **C-trans-keto**, respectively.

Vertical Excited States of the so-optimized clusters were computed at ONIOM QM/QM′ level, with charge embedding (Mulliken charges),[32,53] using the development version of the Gaussian package.[54] The hybrid B3LYP/6-31+G(d) functional (please note that the B3LYP implementation is slightly different between Gaussian and CRYSTAL) was adopted as a high-level method, whereas the HF/3-21+G(d) model was used as low-level approximation. Previous works have demonstrated that the embedding potential obtained at this level of theory is able to accurately simulate the effects related to surrounding environment.[33,55]

Optimizations of the SA molecule in acetonitrile were performed including solvent effects through a Polarizable Continuum Model (PCM).[56] TD-DFT calculations were computed subsequently at the B3LYP/6-31+G(d) level, which is almost as accurate as PBE0 for most organic molecules.[57−59] In such a way, just one exchange functional is used for molecular, cluster, and periodic calculations, allowing for an easier comparison of the results obtained. UV−visible absorption spectra were obtained from the computed vertical excitation energies and oscillator strengths through a Gaussian convolution using a fixed full width at half-maximum (fwhm) of 0.2 eV.

3. RESULTS AND DISCUSSION

The results obtained are discussed here by pursuing the following scheme: first (in Section 3.1) the structural and electronic features of the β polymorph of SA are discussed. Next (in Section 3.2) the results concerning the excited-states properties are exposed, and, finally, some general conclusions on the computational protocols are drawn.

3.1. Structural and Electronic Features of the SA β Polymorph. The β polymorph of crystalline SA (Figure 2) contains 104 atoms in the unit cell (Z = 4). Each molecular unit is present, at the ground state, in its colorless and stable enol-form, which is characterized by an intramolecular H-bond (Figure 2). In the crystal, the enol-form is found to be almost planar, leading to a solid structure that belongs to the orthorhombic $Pbc2_1$ space group, where SA molecules lie along the *b* lattice vector. Moreover, the SA molecules are stacked along the *c* lattice vector, giving rise to a "fishbone"-like pattern that can be illustrated from the *bc* plane view reported in Figure 2.

A full geometry optimization, starting from the experimental structure, was performed at the B3LYP, B3YLP-D2, and B3LYP-D* levels of theory using the 6-311G(d) basis set. The computed cell parameters and volumes are reported in Table 1. It can be observed that the largest differences between the three methods are due to the addition of dispersion-correction terms (either -D2 or -D*), the B3LYP-D* showing a remarkable accuracy with small deviations from the experimental values apart from the *c* lattice vector, which is significantly underestimated (−0.5 Å) at the B3LYP-D* level. This fact is related to the well-known tendency of Grimme's correction to overestimate dispersion interactions.[38,46] Not surprisingly,

dx.doi.org/10.1021/ct500868s | J. Chem. Theory Comput. XXXX, XXX, XXX−XXX

Table 2. Intramolecular and Intermolecular Geometrical Parameters (Å and deg) Computed for the Fully Optimized β Structure of SA and for the Isolated Enol Molecule[c]

		Solid			
		intramolecular parameters			
		B3LYP	B3LYP-D2	B3LYP-D*	exp.[a]
N···H		1.769	1.758	1.757	1.796
N···O		2.652	2.641	2.646	2.639
C−O−H		107.9	107.7	107.4	109.2
C5−C6−N−C7		31.116	8.542	6.955	6.637
O−H		0.991	0.995	0.994	0.963
C−O		1.346	1.348	1.348	1.365
C7−N		1.288	1.289	1.289	1.294
		Solid			
		intermolecular parameters			
type	bond	B3LYP	B3LYP-D2	B3LYP-D*	exp.[a]
H···O	H17···O1	3.388	2.550	2.699	2.909
	H33···O4	5.166	2.463	2.677	2.904
H···π	H23···R1	5.135	3.627	3.786	3.961
	H12···R3	4.288	2.926	3.061	3.323
	H30···R4	3.283	2.419	2.568	2.667
	H21···R4	3.334	2.400	2.532	2.773
	H3···R5	4.234	2.428	2.562	2.774
	H15···R2	4.594	3.546	3.715	3.884
		Gas-Phase			
		intramolecular parameters			
		B3LYP	B3LYP-D2	B3LYP-D*	MP2/6-31G(d,p)[b]
N···H		1.780	1.795	1.779	
N···O		2.656	2.666	2.655	2.641
C−O−H		108.2	108.4	108.1	
C5−C6−N−C7		40.2	37.6	42.10	
C8−C7−N−C6		(177.3)	(177.3)	(177.6)	177.9
O−H		0.988	0.987	0.988	0.990
C−O		1.340	1.341	1.341	1.350
C7−N		1.287	1.287	1.287	1.299

[a]From ref 23. [b]From ref 25. [c]See Figure 2 for atom labeling.

along the *c* axis a greater number of dispersive interactions are present with respect to the two other directions. Such underestimation can also be due to a spurious "attractive" effect arising from the Basis Set Superposition Error (BSSE), which could be sizable with the adopted basis set (6-311G(d)). Consequently, the cell volume is underestimated at the B3LYP-D* level of about −6%, which is indeed less than half of the error associated with B3LYP-D2 calculations (about −14%). Clearly, in the absence of dispersion corrections (i.e., B3LYP result) a large deviation on cell parameters is obtained leading to an important overestimation of the cell volume (more than 43%). Based on these results, only the B3LYP-D* level of theory seems to provide a reasonable description of the geometrical features of such molecular crystals.

For a detailed understanding of the molecular arrangement of SA into the crystal the most relevant computed *intra*-molecular structural parameters are listed in Table 2 and compared with the experimental ones. Overall, small deviations from the experimental values are observed for all these parameters computed by either the -D2 or -D* corrections. Noncovalent N···O and N···H distances seem to be rather accurately described. The largest differences are related to structural parameters that are affected by the crystal packing. This is the case of the C5−C6−N−C7 dihedral angle and of the C−O−H angle (refer to Figure 2 for atom labeling), for which deviations of −0.3° and −1.8° are computed, respectively, at the B3LYP-D* level. B3LYP-D2 provides a larger deviation for C5−C6−N−C7 (+1.9°), an angle which is severely overestimated by B3LYP (+24.5°), providing further evidence for the need of dispersion corrections.

A C5−C6−N−C7 dihedral angle of nearly 7° (at B3LYP-D* level) imposes an almost planar conformation to the SA molecule. Such spatial arrangement of molecular units in the β polymorph is due to the presence of many H···π interactions. These have been monitored to investigate deeply the manifold *inter*molecular interactions, together with two relevant H···O distances. The data values listed in Table 2 show that the optimized structural parameters are reasonably predicted at the B3LYP-D* level, since differences with the available experimental data span from about 0.10 Å to 0.26 Å. All the distances monitored are mildly underestimated because of the H···π interactions: the weak polar character typical of such interactions is, probably, not correctly accounted for by the use of the -D* correction term. Such overestimation of medium/long-range effects could be the main cause for a packing that is more compact than that observed experimentally (as discussed above for predicted cell parameters). This affects also the H···O distances. Not surprisingly, the gas-

dx.doi.org/10.1021/ct500868s | J. Chem. Theory Comput. XXXX, XXX, XXX−XXX

phase intramolecular parameters provided by the three approaches are very similar, except for the C5−C6−N−C7 dihedral angle, presenting variation of only ca. 5°. Indeed, in such a case, long-range effects are minimal, and the contribution of dispersion corrections is negligible. This is also proven by the small deviations obtained using the three methods with respect to previously published high-level MP2/6-31G(d,p) calculations.[25] Of note, the nonplanar conformation obtained for the isolated molecule in gas-phase (with a predicted dihedral angle of about 40°) was somehow expected due to intramolecular steric effects.

Nonetheless, the B3LYP-D* approach appears to be very accurate for the determination of the structural features of SA for all three kinds of structural parameters that were considered, namely (i) the cell parameters, (ii) the main *intra*molecular parameters, and (iii) the *inter*molecular parameters responsible for the crystal packing.

In order to get more insight on the electronic structure of these compounds, the total Density of States (DOS) of the β polymorph was computed and reported in Figure 3, where the population of the highest valence bands (VB) and the bottom conduction bands (CB) are also given.

At the B3LYP-D* level, the β polymorph in the enol-form presents a band gap of 3.50 eV. This value can be compared with the HOMO−LUMO gap of 4.17 eV computed for the relaxed SA molecule in the gas-phase. This difference results both from structural and electronic factors. In order to decouple them, the HOMO−LUMO gap for the isolated molecule kept fixed at the PBC optimized geometry was also calculated. The value obtained (3.97 eV) shows that purely electronic effects, related to the presence of the surrounding molecules, account largely for the modification of the gap (0.47 eV over a total difference of 0.67 eV). This fact clearly underlines the necessity of including closest interacting molecules when aiming at reproducing the ground − or excited − electronic features of this molecular material via a finite−cluster approach and the necessity of explicitly including not only their geometrical but also their electronic effects.

As expected for molecular systems undergoing to ESIPT, the HOMO−LUMO transition (of π−π^* character) responsible for the PT reaction gives rise to a density depletion of the hydroxyl−enolic oxygen atom, thus justifying its increase in acidity at the excited state and, overall, the possibility of an energetically favorable proton transfer reaction. On the other hand, the increase in density at the excited state on the acceptor group (nitrogen atoms) appears, in the present case, to be quite limited. As clearly indicated by the crystalline and molecular orbitals computed for the SA enolic form (reported in the SI), the nature of the MO involved in the ESIPT process is not affected by the presence of the surrounding molecules. Thus, the main influence of the surrounding molecules seems to be on the energetics of the processes but not on its mechanism.

3.2. Absorption Features. In order to evaluate accurately the effect of the surrounding environment on the excited state properties of the SA molecule, the three clusters, hereafter named as **C-enol**, **C-cis-keto**, and **C-trans-keto**, schematically depicted in Figure 4, have been investigated by means of TD-DFT through the use of a QM/QM′ ONIOM model with charge embedding.

The cluster size (15 molecules: 14 explicit molecules of SA treated at low QM′ level, 1 central molecule of SA treated at high QM level) has been chosen based on the network of intermolecular interactions already discussed in Section 3.1. In

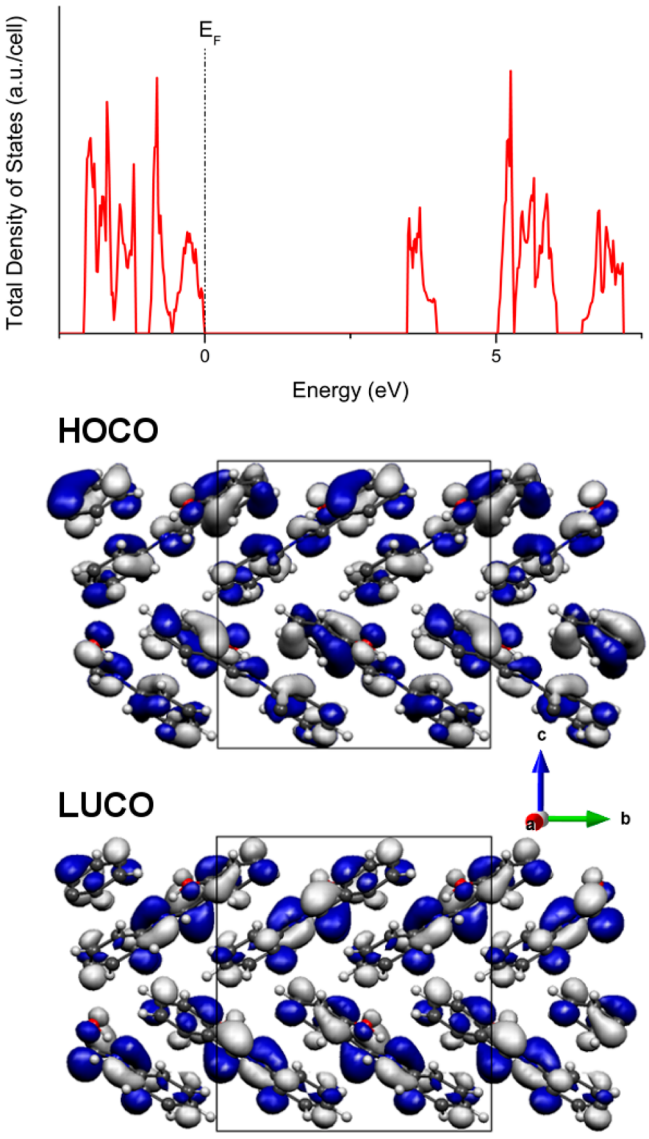

Figure 3. Total density of states (DOS) computed for the fully optimized enol structure of the β polymorph. The top of B3LYP-D* valence bands was set as reference Fermi Energy (E_F = 0). The corresponding γ-point frontier orbitals are also reported (isocontour value 0.02 au).

particular, the molecules considered are related to the central one via intermolecular interactions that span from ca. 2.5 Å to 3.8 Å. Such range can be considered to include all the most relevant H···π, H···O interactions and weaker − van der Waals type − effects. Moreover, we can reasonably assume that the molecules of the low layer form a cage that screens all further interactions that may be envisaged with molecules that are more distant.

The most relevant optimized intramolecular parameters corresponding to the three tautomers of SA obtained for both clusters and isolated molecule are collected in Table 3. Since in this latter case, the dispersion interactions are negligible, the B3LYP-D* data computed for clusters models are compared to the B3LYP results obtained for isolated molecules.

The analysis of the data listed in Table 3 shows that − at a structural level − the embedding in crystal environment only affects the planarity of the molecule. Indeed, within the clusters, the SA molecule presents a quasi-planar conformation

dx.doi.org/10.1021/ct500868s | J. Chem. Theory Comput. XXXX, XXX, XXX−XXX

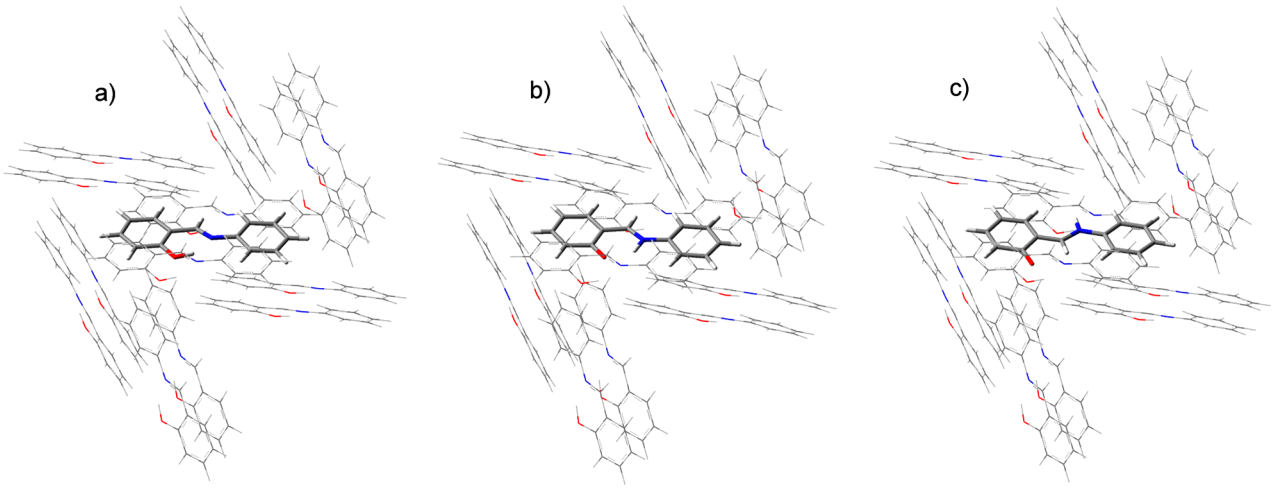

Figure 4. Schematic representation of the C-enol (a), C-cis-keto (b), and C-trans-keto (c) clusters.

Table 3. Intramolecular Geometrical Parameters of the Central Molecule of SA from the Optimized (B3LYP-D*) C-enol, C-cis-keto, and C-trans-keto Clusters, Compared with Isolated Molecules in the Gas-Phase (B3LYP)[a]

	Clusters B3LYP-D* intramolecular parameters		
	C-enol	C-cis-keto	C-trans-keto
N···H/N−H	1.757	1.033	1.014
N···O	2.645	2.645	4.021
C−O−H/C−O···H	107.390	102.982	55.697
C5−C6−N−C7	8.483	2.696	−178.116
O−H/O···H	0.994	1.786	4.684
C−O	1.348	1.266	1.246
C7−N	1.289	1.329	1.335
	Gas-Phase B3LYP intramolecular parameters		
	enol	cis-keto	trans-keto
N···H/N−H	1.780	1.035	1.010
N···O	2.656	2.611	4.095
C−O−H/C−O···H	108.198	103.672	53.767
C5−C6−N−C7	40.165	18.952	−164.720
O−H/O···H	0.988	1.742	4.717
C−O	1.340	1.256	1.233
C7−N	1.287	1.333	1.347

[a]Distances are in Å, angles in deg. For the trans-keto form, the same atoms of enol and cis-keto were considered: distances and angles greatly differ because of the rotation around the C7−N bond (see Figure 2).

independent of the tautomer considered, whereas in the gas-phase a marked nonplanarity of the molecular skeleton is observed.

It is worth noting that, as expected, the **C-enol** form is computed to be the most energetically stable, but the **C-cis-keto** tautomer is predicted to be very close in energy, in agreement with the experimentally observed presence of the cis-keto impurity in SA crystals giving rise to the yellow color.[14] The **C-trans-keto** form, on the other hand, is computed to be sizeably destabilized also due to the enol environment of the surrounding molecules.

From an experimental point of view, the spectra of SA are available both for crystals and in nonpolar solvent (such as isopentane). These spectra are all characterized by a well isolated band attributed to the enol form (at 300−350 nm), red-shifted (in the range of 400−500 nm) in the case of the cis-keto and trans-keto forms.

The UV−visible absorption spectra simulated from the computed TD-DFT vertical electronic excitations energies (listed in the Supporting Information) are depicted in Figure 5, and the most relevant data are collected in Table 4. Overall, the simulated spectra nicely compare with the experiment both in terms of global spectral shape and energy maxima position. Each spectrum presents a characteristic band that can be assigned either to the enol form or to the cis-keto and trans-keto forms. Moreover, even if computed spectra are blue-shifted with respect to the experiment, the relative energy gap between the absorption maxima predicted for the different tautomeric forms is in agreement with experimental results. Such feature further confirms the reliability of the computational protocol adopted in the present work.

By analyzing in more detail the spectra computed for the isolated SA molecule, it can be noticed that the peak (λ_{max}) corresponding to the colorless gas-phase enol form (Figure 5a) is predicted at 336 nm, which nicely compares with the one experimentally measured in isopentane (λ_{max} = 338 nm). Analogously, the cis-keto form of SA, which is produced as thermochromic excitation from the enol form, is predicted to absorb at 413 nm (in the gas-phase, Figure 5b) − the corresponding experimental value in isopentane being 426 nm. Finally, the trans-keto form (in gas-phase) is predicted to absorb at 429 nm (Figure 5c). Unfortunately, in this case, no experimental data for comparison is available.

For all tautomers the λ_{max} corresponds to a vertical excitation from the HOMO to LUMO orbitals (refer to Section S2 in the SI) whose characteristics have been discussed above.

In order to consider the effect of crystal embedding on the vertical excitation energies, let us start by analyzing the spectra computed for the enol form and reported in Figure 5a. These spectra show that the inclusion of the environment produces a sizable red-shift. Indeed, a lower excitation energy is observed for the **C-enol** model, with respect to the gas-phase molecule (336 to 338 nm). Such trend compares well with what is observed experimentally, going from isopentane to solid SA (i.e., from 338 to 340 nm).

The red-shift observed is also somehow qualitatively expected considering the trend discussed for the HOMO−

dx.doi.org/10.1021/ct500868s | J. Chem. Theory Comput. XXXX, XXX, XXX−XXX

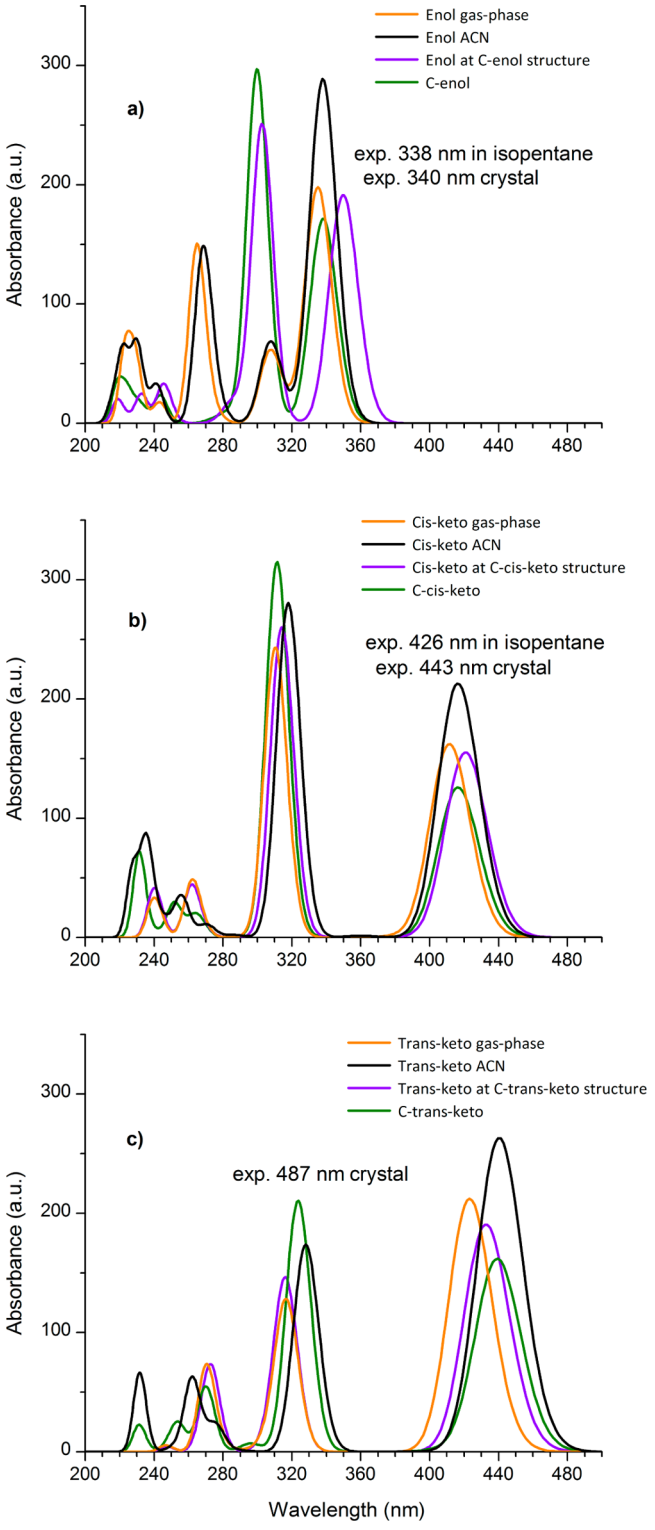

Figure 5. Simulated UV−vis spectra of enol, cis-keto, and trans-keto clusters of β polymorph. The spectra computed for the isolated SA molecule are also reported at the fixed PBC-optimized geometry, the gas-phase geometry, and in acetonitrile solvent. Experimental values for SA in isopentane and crystal are taken from ref 17 and ref 14, respectively.

LUMO gap going from the isolated molecule to the crystal. Indeed, the HOMO−LUMO gap of the gas-phase enol form (4.17 eV) is larger than the one of the isolated molecule at PBC geometry (3.97 eV), thus larger transition energies are expected in the former case.

Table 4. Computed Vertical Absorption Wavelengths (nm) of the Reference Molecule in Different Environments and Structures

	enol	cis-keto	trans-keto
gas-phase	335 (338)[a]	412 (426)[a]	429
ACN	338	416	440
PBC structure	350	421	432
cluster	338 (340)[b]	416 (443)[b]	439 (487)[b]

[a]Experimental data collected in isopentane.[17] [b]Experimental data corresponding to crystal data.[14]

Again, one may question if this red-shift is somehow related to geometric or electronic factors. Figure 5a shows that electronic effects of the surrounding molecules are non-negligible: this is highlighted by the difference of computed λ_{max} between the cluster (338 nm) and the isolated molecule at PBC geometry (350 nm). From this data it clearly appears that if one would consider only the steric effects due to the presence of the environment, the red-shift would be much more marked and the observed behavior is the sum of two − opposite − effects: the structural one − red-shifting − and the electronic one − blue-shifting.

Analogous conclusions can be drawn also for the cis-keto form. In particular, Figure 5b shows that a red-shift of the HOMO−LUMO excitation is observed going from 413 nm (in gas-phase) to 416 nm (in the cluster). The larger deviation − compared with the enol form − observed with respect to the data measured in solid state (443 nm) is indeed related to the fact that the central molecule (in the cis-keto form) is enclosed within a layer of molecules in the enol form. *Strictu sensu* the quantity here computed actually corresponds to the absorption spectra of the "nucleating" cis-keto form more than those of the bulk cis-keto material. Analogously to the enol form, steric and electronic effects due to the presence of the environment play an opposite role: the structural one − red-shifting − and the electronic one − blue-shifting. Contrary to the previous cases, for the trans-keto form both structural and electronic effects, induced by the environment, cause a red-shift in absorption − although structural effects seem to be more relevant than the electronic ones.

4. CONCLUSIONS

The prediction of structural and electronic properties of molecular crystals at the ground and the excited states is a difficult playground for electronic structure methods, due to the need of accurate quantum methods coupled with an efficient description of subtle environmental effects.

In this work, focusing on an experimentally well characterized system, that is the β polymorph of SA, we have shown how the combined use of periodic approaches and embedded cluster ONIOM methods using the same DFT protocol allows for an accurate description of both electronic and structural effects of the crystal on molecular properties. In particular, the effects on the absorption energy of the SA molecule, switching from solution to crystals, has not only been recovered from a quantitative point of view, but its nature has also been analyzed and decomposed in term of structural and/or electronic contributions.

The adopted protocol, though computationally not very expensive, consists of three different steps, namely (i) the

dx.doi.org/10.1021/ct500868s | J. Chem. Theory Comput. XXXX, XXX, XXX−XXX

description of the molecular crystal using a periodic approach accurately taking into account dispersion interactions, (ii) the identification of reliable finite models (clusters), and (iii) the calculation of vertical transition energies including environmental effects through the use of an embedding model (QM/QM′ ONIOM approach).

Overall, the prediction of the properties is rather good, thus encouraging its application to experimentally less characterized molecular crystals.

■ ASSOCIATED CONTENT

Supporting Information

Optimized Cartesian coordinates of clusters used in TD-DFT calculations, HOMOs and LUMOs for different SA molecular tautomers, computed vertical excitations energies for all the species (molecules and embedded clusters). This material is available free of charge via the Internet at http://pubs.acs.org.

■ AUTHOR INFORMATION

Corresponding Authors

*E-mail: alfonso.pedone@unimore.it.
*E-mail: carlo.adamo@chimie-paristech.fr.

Notes

The authors declare no competing financial interest.

■ ACKNOWLEDGMENTS

Computational resources for this work were granted by the "Projet 100339" (2013) at GENCI-IDRIS (Orsay, France). D.P. thanks Regione Emilia-Romagna for financial support through the SPINNER 2013 program entitled 'Ottimizzazione delle forme molecolari e crystalline di farmaci, fitofarmaci, pesticidi in relazione ad attività, biodisponibilità aspetti brevettuali, e alla produzione di polimorfi, solvati e cocrystalli con metodi a basso impatto ambientale'.

■ REFERENCES

(1) El'tsov, A. *Organic Photochromes*; Plenum: New York, 1990.
(2) Ramamurthy, V. *Photochemistry in Organized and Constrained Media*; Wiley-VCH: New York, 1991.
(3) Crano, J. C.; Guglielmetti, R. J. *Organic Photochromic and Thermochromic Compounds*; Topics in Applied Chemistry; Plenum Press: New York, 1999.
(4) Dürr, H.; Bouas-Laurent, H. *Photochromism: Molecules and Systems*, 2nd ed.; Elsevier: Amsterdam, 2003.
(5) Irie, M. Diarylethenes for Memories and Switches. *Chem. Rev.* **2000**, *100*, 1685−1716.
(6) Matsuda, K.; Irie, M. Diarylethene as a Photo Switching Unit. *J. Photochem. Photobiol., C* **2004**, *5*, 169−182.
(7) Senier, A.; Shepheard, F. G. Studies in Phototropy and Thermotropy. Part I. Arylidene- and Naphthylidene-Amines. *J. Chem. Soc., Trans.* **1909**, *95*, 1943−1955.
(8) Senier, A.; Shepheard, F. G.; Clarke, R. Studies in Phototropy and Thermotropy. Part III. Arylideneamines. *J. Chem. Soc., Trans.* **1912**, *101*, 1950−1958.
(9) Ottolenghi, M.; McClure, D. S.; Photochromism, I. The Spectroscopy and Energy Levels of Salicylideneaniline. *J. Chem. Phys.* **1967**, *46*, 4613−4620.
(10) Andes, R. V.; Manikowski, D. M. Photochromism of Salicylidene Aniline. *Appl. Opt.* **1968**, *7*, 1179−1183.
(11) Pasternak, C.; Slifkin, M.; Shinitzky, M. Polarized Photochromism in Solid-Solutions. *J. Chem. Phys.* **1978**, *68*, 2669−2673.
(12) Lewis, J.; Sandorfy, C. A Spectroscopic Study of Proton-Transfer and Photochromism in N-(2-Hydroxybenzylidene)aniline. *Can. J. Chem.* **1982**, *60*, 1738−1746.
(13) Morales, R. G. E.; Jara, G. P.; Vargas, V. Ultraviolet Absorption Bands and Electronic Charge Transfers of Salicylideneanilines in Singlet Excited States. *Spectrosc. Lett.* **2001**, *34*, 1−12.
(14) Fujiwara, T.; Harada, J.; Ogawa, K. Solid-State Thermochromism Studied by Variable-Temperature Diffuse Reflectance Spectroscopy. A New Perspective on the Chromism of Salicylideneanilines. *J. Phys. Chem. B* **2004**, *108*, 4035−4038.
(15) Shen, M. Y.; Zhao, L. Z.; Goto, T.; Mordzinski, A. Polarization Dependence of Photochromism in an N-Salicylideneaniline Single Crystal. *J. Chem. Phys.* **2000**, *112*, 2490−2497.
(16) Sekikawa, T.; Kobayashi, T.; Inabe, T. Femtosecond Fluorescence Study of the Substitution Effect on the Proton Transfer in Thermochromic Salicylideneaniline Crystals. *J. Phys. Chem. A* **1997**, *101*, 644−649.
(17) Ogawa, K.; Harada, J.; Fujiwara, T.; Yoshida, S. Thermochromism of Salicylideneanilines in Solution: Aggregation-Controlled Proton Tautomerization. *J. Phys. Chem. A* **2001**, *105*, 3425−3427.
(18) Vargas, V. Time-Resolved Fluorescence of Salicylideneaniline Compounds in Solution. *J. Phys. Chem. A* **2004**, *108*, 281−288.
(19) Rodríguez-Córdoba, W.; Zugazagoitia, J. S.; Collado-Fregoso, E.; Peon, J. Excited State Intramolecular Proton Transfer in Schiff Bases. Decay of the Locally Excited Enol State Observed by Femtosecond Resolved Fluorescence. *J. Phys. Chem. A* **2007**, *111*, 6241−6247.
(20) Harada, J.; Fujiwara, T.; Ogawa, K. Crucial Role of Fluorescence in the Solid-State Thermochromism of Salicylideneanilines. *J. Am. Chem. Soc.* **2007**, *129*, 16216−16221.
(21) Spörkel, L.; Cui, G.; Thiel, W. Photodynamics of Schiff Base Salicylideneaniline: Trajectory Surface-Hopping Simulations. *J. Phys. Chem. A* **2013**, *117*, 4574−4583.
(22) Destro, R.; Gavezzotti, A.; Simonetta, M. Salicylideneaniline. *Acta Crystallogr., Sect. B: Struct. Crystallogr. Cryst. Chem.* **1978**, *34*, 2867−2869.
(23) Arod, F.; Pattison, P.; Schenk, K. J.; Chapuis, G. Polymorphism in N-Salicylideneaniline Reconsidered. *Cryst. Growth Des.* **2007**, *7*, 1679−1685.
(24) Arod, F.; Gardon, M.; Pattison, P.; Chapuis, G. The α2-Polymorph of Salicylideneaniline. *Acta Crystallogr., Sect. C: Cryst. Struct. Commun.* **2005**, *61*, o317−o320.
(25) Guillaume, M.; Champagne, B.; Markova, N.; Enchev, V.; Castet, F. Ab Initio Investigation on the Second-Order Nonlinear Optical Responses in Keto−Enol Equilibria of Salicylideneanilines. *J. Phys. Chem. A* **2007**, *111*, 9914−9923.
(26) Sekikawa, T.; Schalk, O.; Wu, G.; Boguslavskiy, A. E.; Stolow, A. Initial Processes of Proton Transfer in Salicylideneaniline Studied by Time-Resolved Photoelectron Spectroscopy. *J. Phys. Chem. A* **2013**, *117*, 2971−2979.
(27) Hammes-Schiffer, S.; Stuchebrukhov, A. A. Theory of Coupled Electron and Proton Transfer Reactions. *Chem. Rev.* **2010**, *110*, 6939−6960.
(28) Savarese, M.; Netti, P. A.; Adamo, C.; Rega, N.; Ciofini, I. Exploring the Metric of Excited State Proton Transfer Reactions. *J. Phys. Chem. B* **2013**, *117*, 16165−16173.
(29) Savarese, M.; Netti, P. A.; Rega, N.; Adamo, C.; Ciofini, I. Intermolecular Proton Shuttling in Excited State Proton Transfer Reactions: Insights from Theory. *Phys. Chem. Chem. Phys.* **2014**, *16*, 8661−8666.
(30) Yan, D.; Evans, D. G. Molecular Crystalline Materials with Tunable Luminescent Properties: From Polymorphs to Multi-Component Solids. *Mater. Horiz.* **2013**, *1*, 46−57.
(31) Maseras, F.; Morokuma, K. Imomm - a New Integrated Ab-Initio Plus Molecular Mechanics Geometry Optimization Scheme of Equilibrium Structures and Transition-States. *J. Comput. Chem.* **1995**, *16*, 1170−1179.
(32) Hratchian, H. P.; Parandekar, P. V.; Raghavachari, K.; Frisch, M. J.; Vreven, T. QM:QM Electronic Embedding Using Mulliken Atomic Charges: Energies and Analytic Gradients in an ONIOM Framework. *J. Chem. Phys.* **2008**, *128*, 034107.

(33) García, G.; Ciofini, I.; Fernández-Gómez, M.; Adamo, C. Confinement Effects on UV−Visible Absorption Spectra: B-Carotene Inside Carbon Nanotube as a Test Case. *J. Phys. Chem. Lett.* **2013**, *4*, 1239−1243.
(34) Kamiński, R.; Schmøkel, M. S.; Coppens, P. Constrained Excited-State Structure in Molecular Crystals by Means of the QM/MM Approach: Toward the Prediction of Photocrystallographic Results. *J. Phys. Chem. Lett.* **2010**, *1*, 2349−2353.
(35) Dovesi, R.; Civalleri, B.; Roetti, C.; Saunders, V. R.; Orlando, R. Ab Initio Quantum Simulation in Solid State Chemistry. In *Reviews in Computational Chemistry*; Lipkowitz, K. B., Larter, R., Cundari, T. R., Eds.; John Wiley & Sons, Inc.: 2005; Vol. *21*, pp 1−125.
(36) Corà, F.; Alfredsson, M.; Mallia, G.; Middlemiss, D. S.; Mackrodt, W. C.; Dovesi, R.; Orlando, R. The Performance of Hybrid Density Functionals in Solid State Chemistry. In *Principles and Applications of Density Functional Theory in Inorganic Chemistry II; Structure and Bonding*; Springer: Berlin, Heidelberg, 2004; Vol. *113*, pp 171−232.
(37) Pedone, A.; Presti, D.; Menziani, M. C. On the Ability of Periodic Dispersion-Corrected DFT Calculations to Predict Molecular Crystal Polymorphism in Para-Diiodobenzene. *Chem. Phys. Lett.* **2012**, *541*, 12−15.
(38) Presti, D.; Pedone, A.; Menziani, M. C.; Civalleri, B.; Maschio, L. Oxalyl Dihydrazide Polymorphism: A Periodic Dispersion-Corrected DFT and MP2 Investigation. *CrystEngComm* **2014**, *16*, 102−109.
(39) Presti, D.; Pedone, A.; Menziani, M. C. Unravelling the Polymorphism of [(p-cymene)Ru(kN-INA)Cl2] through Dispersion-Corrected DFT and NMR GIPAW Calculations. *Inorg Chem.* **2014**, *53*, 7926−7935.
(40) Dovesi, R.; Saunders, V. R.; Roetti, C.; Orlando, R.; Zicovich-Wilson, C. M.; Pascale, F.; Doll, K.; Harrison, N. M.; Civalleri, B.; Bush, I. J.; D'Arco, P.; Llunell, M. *CRYSTAL09 User's Manual*; Università di Torino: Torino, 2010.
(41) Dovesi, R.; Orlando, R.; Civalleri, B.; Roetti, C.; Saunders, V. R.; Zicovich-Wilson, C. M. CRYSTAL: A Computational Tool for the Ab Initio Study of the Electronic Properties of Crystals. *Z. Kristallogr.* **2005**, *220*, 571−573.
(42) Becke, A. D. Density-functional Thermochemistry. III. The Role of Exact Exchange. *J. Chem. Phys.* **1993**, *98*, 5648−5652.
(43) Lee, C.; Yang, W.; Parr, R. Development of the Colle-Salvetti Correlation-Energy Formula into a Functional of the Electron-Density. *Phys. Rev. B* **1988**, *37*, 785−789.
(44) Jacquemin, D.; Perpète, E. A.; Ciofini, I.; Adamo, C. Accurate Simulation of Optical Properties in Dyes. *Acc. Chem. Res.* **2009**, *42*, 326−334.
(45) Grimme, S. Semiempirical GGA-Type Density Functional Constructed with a Long-Range Dispersion Correction. *J. Comput. Chem.* **2006**, *27*, 1787−1799.
(46) Civalleri, B.; Zicovich-Wilson, C. M.; Valenzano, L.; Ugliengo, P. B3LYP Augmented with an Empirical Dispersion Term (B3LYP-D*) as Applied to Molecular Crystals. *CrystEngComm* **2008**, *10*, 405−410.
(47) Grimme, S.; Antony, J.; Ehrlich, S.; Krieg, H. A Consistent and Accurate Ab Initio Parametrization of Density Functional Dispersion Correction (DFT-D) for the 94 Elements H-Pu. *J. Chem. Phys.* **2010**, *132*, 154104.
(48) Tkatchenko, A.; Scheffler, M. Accurate Molecular Van Der Waals Interactions from Ground-State Electron Density and Free-Atom Reference Data. *Phys. Rev. Lett.* **2009**, *102*, 073005.
(49) Schatschneider, B.; Liang, J.-J.; Reilly, A. M.; Marom, N.; Zhang, G.-X.; Tkatchenko, A. Electrodynamic Response and Stability of Molecular Crystals. *Phys. Rev. B* **2013**, *87*, 060104.
(50) Otero-de-la-Roza, A.; Johnson, E. R. Van Der Waals Interactions in Solids Using the Exchange-Hole Dipole Moment Model. *J. Chem. Phys.* **2012**, *136*, 174109.
(51) Krishnan, R.; Binkley, J.; Seeger, R.; Pople, J. Self-Consistent Molecular-Orbital Methods 0.20. Basis Set for Correlated Wave-Functions. *J. Chem. Phys.* **1980**, *72*, 650−654.
(52) Peintinger, M. F.; Oliveira, D. V.; Bredow, T. Consistent Gaussian Basis Sets of Triple-Zeta Valence with Polarization Quality for Solid-State Calculations. *J. Comput. Chem.* **2013**, *34*, 451−459.
(53) Parandekar, P. V.; Hratchian, H. P.; Raghavachari, K. Applications and Assessment of QM:QM Electronic Embedding Using Generalized Asymmetric Mulliken Atomic Charges. *J. Chem. Phys.* **2008**, *129*, 145101.
(54) Frisch, M. J.; Trucks, G. W.; Schlegel, H. B.; Scuseria, G. E.; Robb, M. A.; Cheeseman, J. R.; Scalmani, G.; Barone, V.; Mennucci, B.; Petersson, G. A.; Nakatsuji, H.; Caricato, M.; Li, X.; Hratchian, H. P.; Izmaylov, A. F.; Bloino, J.; Zheng, G.; Sonnenberg, J. L.; Liang, W.; Hada, M.; Ehara, M.; Toyota, K.; Fukuda, R.; Hasegawa, J.; Ishida, M.; Nakajima, T.; Honda, Y.; Kitao, O.; Nakai, H.; Vreven, T.; Montgomery, J. A., Jr.; Peralta, J. E.; Ogliaro, F.; Bearpark, M.; Heyd, J. J.; Brothers, E.; Kudin, K. N.; Staroverov, V. N.; Keith, T.; Kobayashi, R.; Normand, J.; Raghavachari, K.; Rendell, A.; Burant, J. C.; Iyengar, S. S.; Tomasi, J.; Cossi, M.; Rega, N.; Millam, J. M.; Klene, M.; Knox, J. E.; Cross, J. B.; Bakken, V.; Adamo, C.; Jaramillo, J.; Gomperts, R.; Stratmann, R. E.; Yazyev, O.; Austin, A. J.; Cammi, R.; Pomelli, C.; Ochterski, J. W.; Martin, R. L.; Morokuma, K.; Zakrzewski, V. G.; Voth, G. A.; Salvador, P.; Dannenberg, J. J.; Dapprich, S.; Parandekar, P. V.; Mayhall, N. J.; Daniels, A. D.; Farkas, O.; Foresman, J. B.; Ortiz, J. V.; Cioslowski, J.; Fox, D. J. *GAUSSIAN09 Development Version H.32*; Gaussian, Inc.: Wallingford, CT, 2010.
(55) Labat, F.; Ciofini, I.; Hratchian, H. P.; Frisch, M.; Raghavachari, K.; Adamo, C. First Principles Modeling of Eosin-Loaded ZnO Films: A Step toward the Understanding of Dye-Sensitized Solar Cell Performances. *J. Am. Chem. Soc.* **2009**, *131*, 14290−14298.
(56) Corni, S.; Cammi, R.; Mennucci, B.; Tomasi, J. Electronic Excitation Energies of Molecules in Solution within Continuum Solvation Models: Investigating the Discrepancy between State-Specific and Linear-Response Methods. *J. Chem. Phys.* **2005**, *123*, 134512.
(57) Barone, V.; Biczysko, M.; Bloino, J.; Carta, L.; Pedone, A. Environmental and Dynamical Effects on the Optical Properties of Molecular Systems by Time-Independent and Time-Dependent Approaches: Coumarin Derivatives as Test Cases. *Comput. Theor. Chem.* **2014**, *1037*, 35−48.
(58) Jacquemin, D.; Perpète, E. A.; Ciofini, I.; Adamo, C.; Valero, R.; Zhao, Y.; Truhlar, D. G. On the Performances of the M06 Family of Density Functionals for Electronic Excitation Energies. *J. Chem. Theory Comput.* **2010**, *6*, 2071−2085.
(59) Caricato, M. Exploring Potential Energy Surfaces of Electronic Excited States in Solution with the EOM-CCSD-PCM Method. *J. Chem. Theory Comput.* **2012**, *8*, 5081−5091.